Biochimica et Biophysica Acta 1842 (2014) 135–143

Contents lists available at ScienceDirect

Biochimica et Biophysica Acta

journal homepage: www.elsevier.com/locate/bbadis

Suppression of tumorigenesis in mitochondrial NADP$^+$-dependent isocitrate dehydrogenase knock-out mice

Seontae Kim [a], Sung Youl Kim [a], Hyeong Jun Ku [a], Yong Hyun Jeon [b], Ho Won Lee [b], Jaetae Lee [b], Taeg Kyu Kwon [c], Kwon Moo Park [d], Jeen-Woo Park [a,*]

[a] School of Life Sciences and Biotechnology, College of Natural Sciences, Kyungpook National University, Taegu 702-701, Republic of Korea
[b] Department of Nuclear Medicine, School of Medicine, Kyungpook National University, Taegu 700-422, Republic of Korea
[c] Department of Immunology, College of Medicine, Keimyung University, Taegu 700-712, Republic of Korea
[d] Department of Anatomy, School of Medicine, Kyungpook National University, Taegu 700-422, Republic of Korea

ARTICLE INFO

Article history:
Received 25 July 2013
Received in revised form 14 October 2013
Accepted 8 November 2013
Available online 12 November 2013

Keywords:
Antioxidant enzyme
Knockout mice
Tumorigenesis
Redox status
Host microenvironment

ABSTRACT

The tumor host microenvironment is increasingly viewed as an important contributor to tumor growth and suppression. Cellular oxidative stress resulting from high levels of reactive oxygen species (ROS) contributes to various processes involved in the development and progress of malignant tumors including carcinogenesis, aberrant growth, metastasis, and angiogenesis. In this regard, the stroma induces oxidative stress in adjacent tumor cells, and this in turn causes several changes in tumor cells including modulation of the redox status, inhibition of cell proliferation, and induction of apoptotic or necrotic cell death. Because the levels of ROS are determined by a balance between ROS generation and ROS detoxification, disruption of this system will result in increased or decreased ROS level. Recently, we demonstrated that the control of mitochondrial redox balance and cellular defense against oxidative damage is one of the primary functions of mitochondrial NADP$^+$-dependent isocitrate dehydrogenase (IDH2) that supplies NADPH for antioxidant systems. To explore the interactions between tumor cells and the host, we evaluated tumorigenesis between IDH2-deficient (knock-out) and wild-type mice in which B16F10 melanoma cells had been implanted. Suppression of B16F10 cell tumorigenesis was reproducibly observed in the IDH2-deficient mice along with significant elevation of oxidative stress in both the tumor and the stroma. In addition, the expression of angiogenesis markers was significantly down-regulated in both the tumor and the stroma of the IDH2-deficient mice. These results support the hypothesis that redox status-associated changes in the host environment of tumor-bearing mice may contribute to cancer progression.

1. Introduction

Tumor growth, invasion, and metastasis depend not only on the tumor cells but also on the complex interactions between the tumor cells and host [1]. The tumor host microenvironment is increasingly viewed as an important contributor to tumor growth and suppression [2]. Most human carcinomas arise from neoplastic epithelial cells that coexist with a variety of extracellular matrix components and cell types, notably fibroblasts, myofibroblasts, adipocytes, endothelial cells, pericytes, and immune cells, that collectively form the tumor stroma [3–5]. Several lines of evidence have demonstrated that the tumor stroma influences the growth, survival, invasiveness, and metastatic ability of the neoplastic epithelial cells within these tumors [6,7]. Cellular oxidative stress resulting from high levels of reactive oxygen species (ROS) contributes to various processes involved in malignant tumor growth and progression including carcinogenesis, aberrant growth, metastasis, and angiogenesis. Since ROS are usually increased in cancer cells and ROS do involve in initiation, progression and metastasis of cancers, ROS are considered oncogenic [8]. On the other hand, high levels of ROS, which can be achieved by various anti-cancer treatments, suppress tumor metastasis by destroying cancer cells due to the oxidative nature of ROS [9]. In this regard, the stroma induces oxidative stress in adjacent tumor cells that in turn causes several changes in tumor cells including modulation of the redox status, inhibition of cell proliferation, and induction of apoptotic or necrotic cell death.

Because the level of ROS is determined by a balance between ROS generation and ROS detoxification, changes in this system will result in increased or decreased ROS levels. Not only increased ROS production but also reduced ROS detoxification has been observed in conjunction with tumor growth and metastasis [9]. Biological systems have evolved an effective and complicated network of defense mechanisms that enable cells to cope with lethal oxidative environments. These defense mechanisms involve antioxidant enzymes such as superoxide dismutase (SOD), catalase, and peroxidases [10]. Mitochondrial manganese SOD (MnSOD) [11] and glutathione peroxidase [12] serve as primary defenses against ROS in mitochondria. Reduced glutathione (GSH)

* Corresponding author. Tel.: +82 53 950 6352; Fax: +82 53 943 2762.
E-mail address: parkjw@knu.ac.kr (J.-W. Park).

0925-4439/$ – see front matter © 2013 Elsevier B.V. All rights reserved.
http://dx.doi.org/10.1016/j.bbadis.2013.11.008

participates in the defense against ROS both as a potent antioxidant and substrate for mitochondrial glutathione peroxidase and glutathione-dependent phospholipid hydroperoxidase [13]. GSH levels in mitochondria are maintained by NADPH-dependent glutathione reductase [14]. NADPH is also required for the regeneration of the thioredoxin system that is essential for maintaining cellular thiol homeostasis [15]. Thus, mitochondrial NADPH is fundamentally important for the defense against ROS.

The isocitrate dehydrogenases (ICDHs; EC1.1.1.41 and EC1.1.1.42) catalyze oxidative decarboxylation of isocitrate into α-ketoglutarate, and require either NAD^+ or $NADP^+$ to produce NADH and NADPH, respectively [16]. In mammals, there are three classes of ICDH isoenzymes represented by mitochondrial NAD^+-dependent ICDH, mitochondrial $NADP^+$-dependent ICDH (IDPm or IDH2), and cytosolic $NADP^+$-dependent ICDH (IDPc or IDH1) [16]. We reported that IDH2 helps supply NADPH needed for GSH production that confers protection against mitochondrial oxidative damage [17]. In particular, IDH2 plays a very important part in the cellular defense against oxidative stress by providing NADPH in the mitochondria since glucose 6-phosphate dehydrogenase (G6PD) is not found in mitochondria [17]. Considering the cytoprotective role of IDH2 and potential vulnerability of the metastatic microenvironment to oxidative stress, we speculated that tumorigenesis may be suppressed in IDH2-deficient mice. In addition, the role of IDH2 in reductive carboxylation glutaminolysis which is responsible for tumor survival has been proposed [18].

To explore the interactions between tumor cells and the host, we monitored tumorigenesis in IDH2-deficient (knock-out, $idh2^{-/-}$) and wild-type ($idh2^{+/+}$) mice in which B16F10 melanoma cells had been implanted. Tumorigenesis of the B16F10 cells was reproducibly suppressed in the IDH2-deficient mice while oxidative stress in both the tumor and the stroma was significantly elevated. These results support the hypothesis that changes associated with redox status in the host environment of tumor-bearing mice may contribute to cancer progression.

2. Materials and methods

2.1. Materials

β-$NADP^+$, isocitrate, xylenol orange, 2,4-dinitophenylhydrazine (DNPH), and 5,5′-dithiobis(2-nitrobenzoic acid) (DTNB) were obtained from Sigma Chemical Co. (St. Louis, MO). Antibodies were purchased from Santa Cruz Biotechnology (Santa Cruz, CA) or Cell Signaling (Beverly, MA). A peptide containing the 16 N-terminal amino acids of mouse IDH2 (ADKRIKVAKPVVEMPG) was used to prepare polyclonal anti-IDH2 antibodies [17].

2.2. Establishment of a stable cell line expressing the firefly luciferase (Fluc) gene

B16F10 mouse melanoma cells were grown in Dulbecco's modified Eagle's medium supplemented with 10% (v/v) fetal bovine serum, 100 units/mL penicillin, and 100 μg/mL streptomycin at 37 °C in a 5% CO_2/95% humidified atmosphere. The B16F10 cells were grown to 70–80% confluency before being transfected with a recombinant lentivirus bearing a plasmid containing both the firefly luciferase (Fluc) and green fluorescent protein (GFP) genes driven by a CMV promoter (pLenti/CMV-Fluc-IRES-GFP). After transfection, the B16F10 cells were cultured for several days and expression of the plasmid was monitored according to the GFP signals with fluorescent microscopy (Nikon Eclipse Ti-S; Nikon Inc., Japan). Cells that expressed Fluc and GFP proteins were selected by flow cytometry (FACSorter; BD Biosciences, San Jose, CA).

2.3. Generation and characterization of idh2 knock-out mice

Genomic DNA was extracted from 129/SvJ mouse J1 embryonic stem cells and was used as template DNA for PCR. A targeting vector was constructed to delete a 1170-bp genomic fragment containing a segment of the N-terminal region of the *idh2* gene using a 5′ 7.3-kb long arm fragment and 3′ 2.4-kb short arm fragment ligated into a pPNT vector. The neomycin phosphotransferase gene (neo) that conferred resistance to the neomycin analog, G418, was used for positive selection. Herpes simplex virus thymidine kinase (HSVtk), which conferred sensitivity to the guanine analog, ganciclovir (GANC), was used for negative selection. The targeting vector was linearized with Not1 and used to transfect 129/SvJ mouse J1 embryonic stem cells via electroporation. Clones resistant to G418 and GANC were selected, and homologous recombination was confirmed by Southern blotting. Among the 35 clones obtained, the *idh2* gene was successfully modified in five. To produce chimeric mice, embryonic stem clones containing the targeted mutation were injected into C57BL/6 blastocysts that were subsequently transferred to recipient female mice on day 3 of pseudo-pregnancy. The resulting male chimeric mice were bred with C57BL/6 females to obtain heterozygous *idh2* mice. Germline transmission of the mutant allele was verified by Southern blot analysis of tail DNA from F1 offspring with agouti coat color. The heterozygous mice were interbred to generate homozygous *idh2*-deficient mice. For Southern blot analysis, a 1-kb probe located just outside the 3′ short arm of the knock-out vector was prepared using two primers (forward primer, 5′-TGCCTCCACCTTCTTAGTAGG-3′; reverse primer, 5′-ACTAACGGATGGCATCAGCAG-3′). Mouse genomic DNA was isolated from mouse tail samples, digested with SphI, and hybridized with the probe.

2.4. Animal protocol

Animal studies were conducted in accordance with the institutional guidelines for the care and use of laboratory animals. B16F10 cells (1×10^5/0.1 mL PBS) were subcutaneously injected into the right thigh of C57BL/6 wild-type (WT) and *idh2* knock-out (KO) mice that were divided into four groups (WT, WT + 5 Gy, KO, and KO + 5 Gy) containing 5–6 mice in each group. Tumor volumes were measured every 2 days and calculated (in mm^3) according to the formula: short $size^2 \times$ long size / 2. The animals were euthanized 1 week after receiving whole body irradiation with a ^{137}Cs source at a dose rate of 1 Gy/min. Primary tumors in the flank were excised, snap-frozen in liquid nitrogen, and stored at −80 °C.

2.5. Preparation of tissue extracts

Tissues from the mice were homogenized with a solution containing 0.3 M sucrose, 25 mM imidazole, 1 mM EDTA (pH 7.2), 8.5 μM leupeptin, and 100 μg/mL aprotinin using a homogenizer at maximum speed for 15 s. Each homogenate was then centrifuged at 4000 ×*g* for 15 min at 4 °C. The resulting supernatants were stored at −20 °C before use. The protein concentrations were measured by the Bradford method using reagents purchased from Bio-Rad (Hercules, CA).

2.6. Bioluminescence imaging analysis

Bioluminescence imaging of the mice was performed using an IVIS Lumina II (Caliper Life Sciences, Hopkinton, MA) with a highly sensitive CCD camera mounted on a light-tight specimen chamber. D-luciferin potassium salt (Caliper Life Sciences, Hopkinton, MA) was diluted to 3 mg/100 μL in PBS before use, and 100 μL of this solution was injected intraperitoneally into the mice. After 10 min, the mice were placed individually in the specimen chamber and light emitted by the luciferase was measured. Grayscale photographic images and bioluminescent color images were superimposed using LIVINGIMAGE, version 2.12 (Xenogen, Alameda, CA), and IGOR image analysis FX software

(WaveMetrics, Lake Oswego, OR). Bioluminescence signals are expressed in units of photons per cm^2 per second per steradian ($P/cm^2/s/sr$). To quantify the emitted light, regions of interest (ROIs) were drawn over the tumor region and total photon efflux over an exposure time of 1 s was evaluated.

2.7. RNA isolation and reverse transcription (RT)-PCR

RNA was isolated using an RNeasy kit (Qiagen, Hilden, Germany) according to the manufacturer's instruction. Total RNA (1 μg) was reverse-transcribed into cDNA using a first-strand cDNA synthesis kit (Invitrogen, Carlsbad, CA) according to the manufacturer's protocol. The cDNA template was then amplified by RT-PCR using a Perkin–Elmer GeneAmp PCR System 2400 (Perkin–Elmer Cetus, Waltham, MA) according to the manufacturer's protocol. Sequences of the primers used were as follows: *β-actin*, forward 5′-TCTACAATGAGCTGCGTGTG-3′, reverse 5′-ATCTCCTTCTGCATCCT-GTC-3′; *IDH2*, forward 5′-ATCAAGGA GAAGC-TCATCCTGC-3′, reverse 5′-TCTGTGGCCTTGTACTGGTCG-3′; vascular endothelial growth factor (*VEGF*) forward 5′-ACTTGTGTTGGGAG GAGGATGTC-3′, reverse 5′- AATGGGTTTGTCGTGTTTCTGG-3′; *HIF-1α*, forward 5′- TCATCAGTTGCCACTTCCCCAC-3′, reverse 5′- CCGTCATCTG TTAGCACCATCAC-3′; *Glut-1*, forward 5′- GACCCTGCACCTCATTGG -3′, reverse 5′- GATGCTCAGATAGGACATCCAAG -3′; *βFGF*, forward 5′-CCCGAC GGCCGCGTGGAT-3′, reverse 5′- ACTTAGAAGCCAGCAGCCG-3′. β-Actin was used as an internal control. Each PCR reaction contained 1× SYBR Premix Ex Taq, 0.2 μM of each primer, and 2 μL of a 1:5 dilution of the cDNA in a final volume of 20 μL. The following PCR program was used for amplification: initial denaturation at 95 °C for 10 s followed by 40 cycles of 95 °C for 5 s, and 60 °C for 20 s with a temperature transition rate of 20 °C/s. The amplified DNA products were resolved on a 1% agarose gel and stained with ethidium bromide. For the melting curve analysis, the PCR reactions were denatured at 95 °C and reannealed at 65 °C. Release of the intercalator from the PCR products or primer dimers was then monitored by increasing the temperature to 95 °C with at a rate of 0.1 °C/s. To create a standard curve, homologous standards for each gene were used as external standards for all experiments. cDNA was quantified using the second derivative maximum methods of Light Cycler Software ver. 4.0 (Roche Diagnostics, Indianapolis, IN).

2.8. Immunoblot analysis

Proteins were separated in an 8–12.5% SDS-polyacrylamide gel, transferred to nitrocellulose membranes, and subsequently subjected to immunoblot analysis using the appropriate antibodies. Antibody binding was then detected with an enhanced chemiluminescence detection kit (Amersham Pharmacia Biotech, Buckinghamshire, UK). Analysis of the blot images was performed with ImageJ software using the "Gel Analysis" function.

2.9. Measurement of cellular redox status and oxidative damage

NADPH was measured using the enzymatic cycling method as described previously [17] and expressed as the ratio of NADPH to the total NADP pool. Intracellular H_2O_2 concentrations were measured

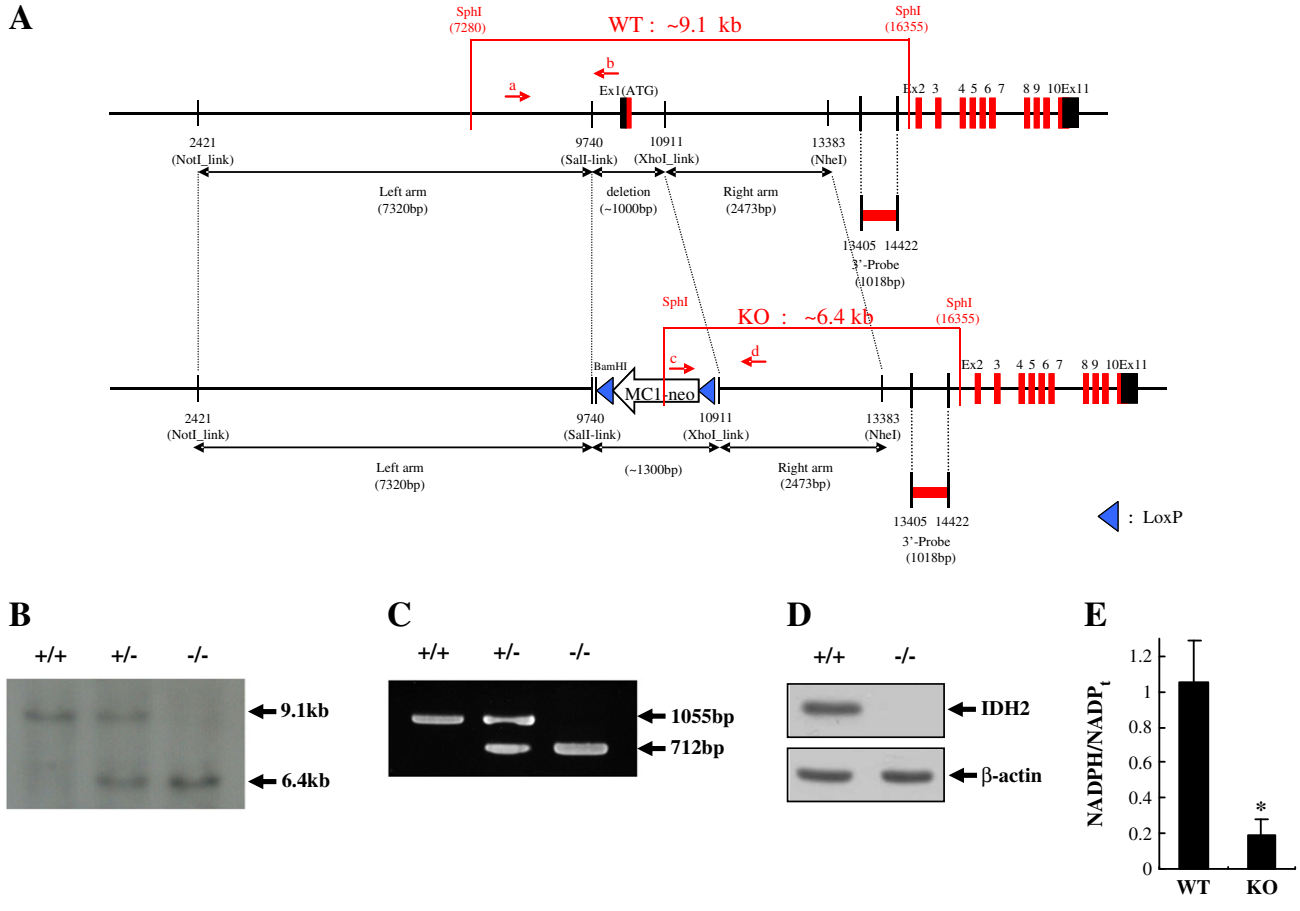

Fig. 1. Generation and characterization of IDH2 knock-out mice. (A) Structure of the *idh2* genome locus and targeting construct. The targeting vector was used to delete ~1170 bp of genomic DNA, including the presumed *idh2* promoter and ATG start codon (neo, neomycin resistance gene; a, wild-type sense primer; b, wild-type antisense primer; c, knock-out sense primer; d, knock-out antisense primer). (B) Genotyping by Southern blotting. Genomic DNA was extracted from the tails of $idh2^{+/+}$ (WT), $idh2^{+/-}$ (hetero), and $idh2^{-/-}$ (KO) mice, digested with Sph1, and hybridized with a 3′-probe (1018 bp). (C) RT-PCR analysis of gene expression in WT, hetero, and KO mice. (D) Expression of IDH2 protein identified by immunoblotting using an anti-IDH2 antibody. β-Actin was used as a loading control. (E) Ratio of NADPH versus the total NADPH pool. Each value represents the mean ± S.D. from five or six independent experiments. $^*p < 0.01$ versus the $idh2^{+/+}$ mice.

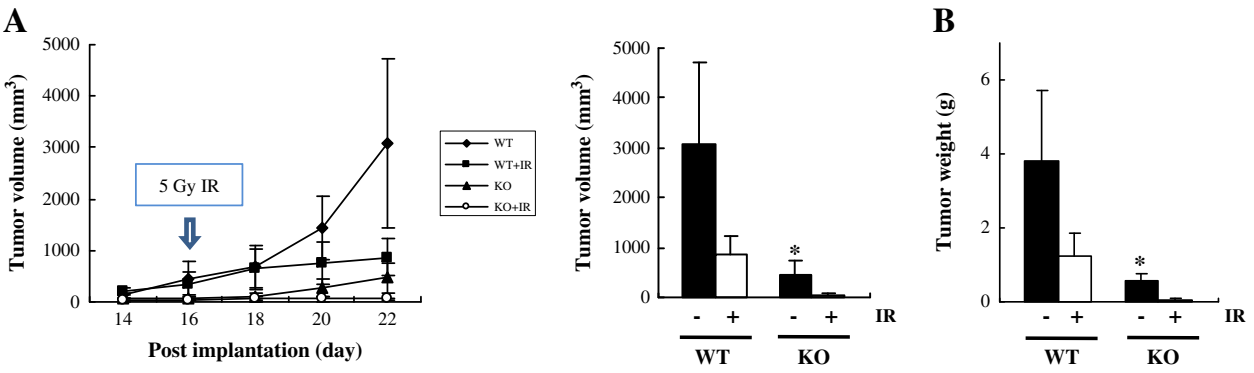

Fig. 2. B16F10 melanoma growth in IDH2 knock-out mice. (A) Growth curve showing the average melanoma size for each group. Tumor volumes were measured with a digital caliper every 2 days. Tumor volume (mm^2) was calculated with the formula: short $size^2$ × long size / 2. Each value represents the mean ± S.D. from five or six independent experiments. (B) Average tumor volumes for the $idh2^{+/+}$ and $idh2^{-/-}$ mice exposed to 5 Gy of ionizing radiation (IR). Tumor volumes were determined at the time of sacrifice. Each value represents the mean ± S.D. from five or six independent experiments. *$p < 0.01$ versus the non-irradiated $idh2^{+/+}$ mice. (C) Average tumor weights for the $idh2^{+/+}$ and $idh2^{-/-}$ mice exposed to 5 Gy of IR. Tumor weights were determined at the time of sacrifice. Each value represents the mean ± S.D. from five or six independent experiments. *$p < 0.01$ versus the non-irradiated $idh2^{+/+}$ mice.

using a ferric sensitive dye, xylenol orange, as previously described [19]. A Protein Carbonyl Assay Kit (Cayman Chemical, Ann Arbor, MI) was used to measure protein carbonyl contents in the cell lysates. This kit measured the reaction between DNPH and protein carbonyls. The amount of protein-hydrazone produced was quantified spectrophotometrically at an absorbance between 360 and 385 nm. The carbonyl content was then standardized to determine the protein concentration. The protein carbonyl content was also determined immunochemically using OxyBlot Protein Oxidation Detection Kit (Millipore, Billerica, MA). The levels of thiobarbituric acid-reactive substances (TBARS) were determined as an independent measurement of lipid peroxidation. Tissue homogenates (500 μL) were mixed with 1 mL TBA solution

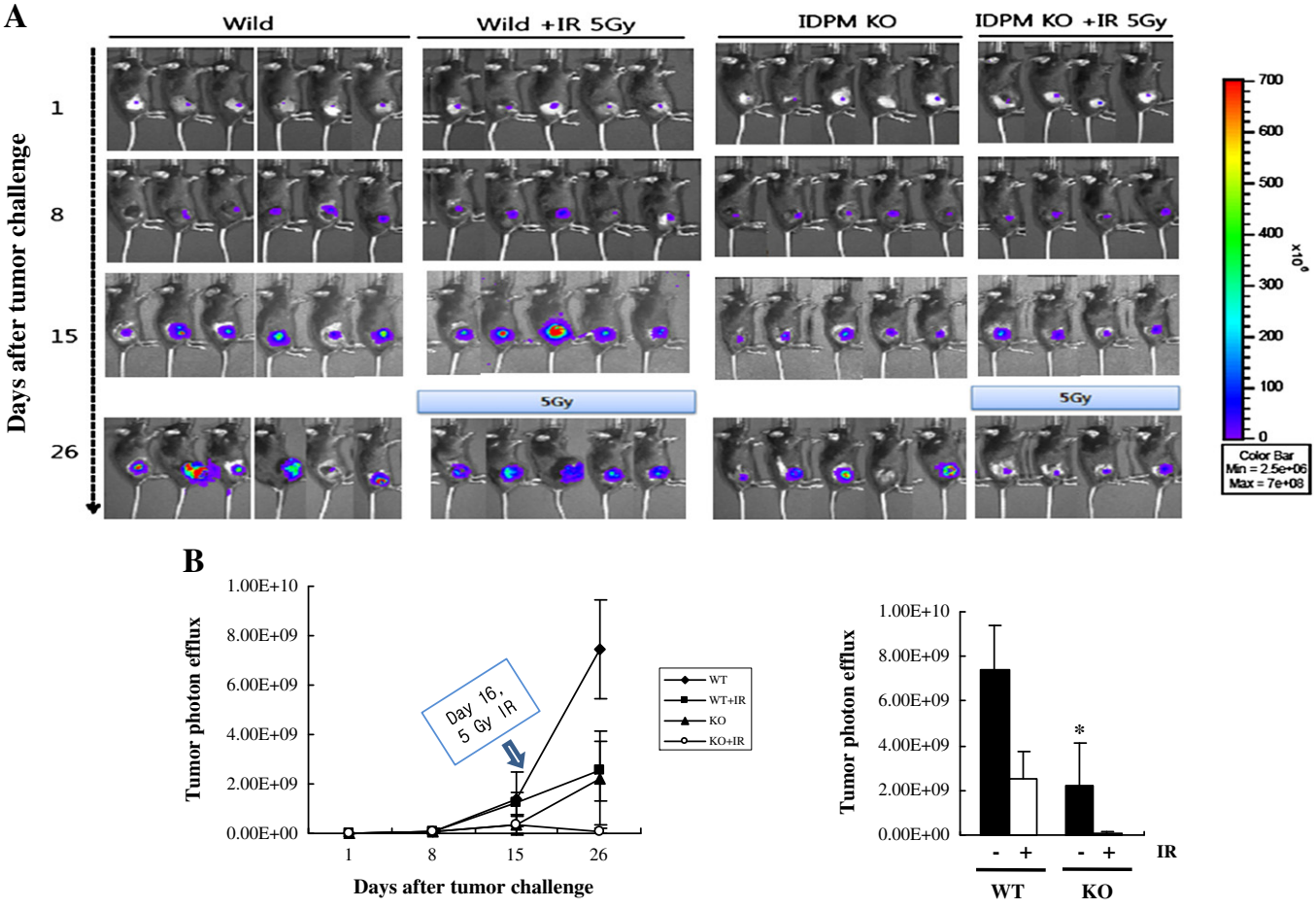

Fig. 3. The effect of IDH2 deficiency on the growth of B16F10 melanoma cells in vivo. (A) Representative bioluminescence images of the $idh2^{+/+}$ and $idh2^{-/-}$ mice recorded after subcutaneous inoculation with B16F10 cells expressing GFP and Fluc genes. (B) Bioluminescence intensity quantified according to regions of interest (ROIs) that encompassed the tumor. Each value represents the mean ± S.D. from four to six independent experiments. (C) Quantification of bioluminescence intensity at the time of sacrifice. Each value represents the mean ± S.D. from four to six independent experiments. *$p < 0.01$ versus non-irradiated $idh2^{+/+}$ mice.

(0.375% thiobarbituric acid in 0.25 N HCl containing 15% [w/w] trichloroacetic acid) and heated at 100 °C for 15 min. The reaction was then stopped by incubating on ice, and the absorbance was measured at 535 nm. Malondialdehyde (MDA) production in the samples was evaluated using a spectrophotometric assay for TBARS as previously described [20]. Lipid peroxidation in tissues was also measured with anti-HNE Michael adduct antibody after SDS-PAGE as previously described [21].

2.10. 2-DE, in-gel tryptic digestion, and protein identification by mass spectrometry (MS)

2-DE was performed with an Ettan IPGphor Isoelectric Focusing (IEF) System (Amersham Pharmacia Biotech) using 24 cm, pH 4–10 nonlinear and pH 4–7 Immobiline Dry Strips for first-dimensional separation, and 10–16% SDS-polyacrylamide gradient gels for the second dimension. SDS-PAGE was performed in an Ettan DALTsix Large Vertical System (Amersham Pharmacia Biotech). Spots of interest were excised and in-gel digestion was subsequently performed with 20 mL of 50 mM H_4HCO_3 (pH 8.0) containing 20 mg/mL trypsin (Promega, Madison, WI). MALDI-TOF MS was performed using an Applied Biosystems 4700 proteomics analyzer (Applied Biosystems, Foster City, CA) in the reflector/delayed-extraction mode. Proteins were identified according to peptide mass fingerprint (PMF) using the Swiss-Prot (updated 30/03/2010) and NCBInr (updated 30/03/2010) databases with a special search tool [MS-FIT from Protein Prospector V 5.6.1 (http://prospector.ucsf.edu)].

2.11. Measurement of serum VEGF with an ELISA

Mice were euthanized and blood was obtained by cardiac puncture. Serum was recovered from the blood by centrifugation in a BD Microtainer SST Tube at 10,000 ×*g* for 90 s. VEGF concentrations in the serum (50 μL) were analyzed using a mouse VEGF ELISA kit (Quantikine R & D Systems, Minneapolis, MN) according to the manufacturer's protocol.

2.12. Statistical analysis

Differences between two mean values were analyzed by Student's *t*-test. *p*-Values < 0.05 were considered to be statistically significant.

2.13. Replicates

Unless otherwise indicated, all results described in this paper are representative of at least three separate experiments.

3. Results and discussion

3.1. Identification of IDH2 knock-out mice

IDPm plays an essential role in cellular defense against oxidative damage by supplying NADPH in the mitochondria. NADPH is a required cofactor for the regeneration of GSH, the most abundant low molecular mass thiol in most organisms, by glutathione reductase along with its critical role in the NADPH-dependent thioredoxin system [14,15]. Mitochondrial GSH plays a key part in protection against ROS-mediated damage because this factor not only functions as a potent antioxidant but is also required for the activities of mitochondrial glutathione peroxidase and mitochondrial phospholipid hydroperoxide glutathione peroxidase [22] that removes mitochondrial peroxides. The oxidized form of thioredoxin that contains a disulfide bridge between the half-cystines can be reduced by NADPH in the presence of thioredoxin reductase, a flavoprotein [23]. Reduced thioredoxin may provide reducing equivalents to mitochondrial thioredoxin peroxidase/peroxiredoxin family members including peroxiredoxin III/protein SP-22 [24–26] and peroxiredoxin V/AOEB166 [27]. In this regard, elevation of mitochondrial NADPH and GSH by IDH2 reduces oxidative stress and suppresses concomitant ROS-mediated cell death. To obliterate IDH2 gene expression, a specific part of the gene was removed and replaced with an artificial piece of DNA (Fig. 1A). ES clones containing the mutant IDH2 gene were obtained and IDPm knock-out mice were produced as confirmed by Southern blot analysis. A 9.1-kb *idh2* wild-type ($idh2^{+/+}$) DNA fragment and 6.4-kb *idh2* mutant ($idh2^{-/-}$) DNA fragment were detected (Fig. 1B). An absence of mRNA and protein expression in the $idh2^{-/-}$ animals was observed with RT-PCR (Fig. 1C) and Western blot analysis (Fig. 1D), respectively. The major 47-kDa protein band was detected in the wild-type mice whereas the band was not present in the knock-out mice. The ratio for mitochondrial [NADPH]/[$NADP^+$/NADPH] was significantly decreased in the tissues of $idh2^{-/-}$ mice compared to that from $idh2^{+/+}$ mice (Fig. 1E).

3.2. B16F10 melanoma cell growth in IDH2 knock-out mice

To determine whether IDH2 deficiency suppresses tumor growth in vivo, $idh2^{+/+}$ and $idh2^{-/-}$ age-matched male mice were subcutaneously inoculated with B16F10 cells, a highly metastatic malignant melanoma cell line. Fig. 2 shows that melanoma tumor growth was suppressed in the IDH2 knock-out animals, resulting a 5.8-fold decrease in tumor volume and 7.2-fold decrease in tumor mass relative to the wild-type mice. Thus, an IDPm-deficient tumor environment provided inhospitable conditions for melanoma tumor growth.

Radiation therapy has been commonly used to treat tumors. Ionizing radiation (IR) has been shown to generate ROS in a variety of cells [28].

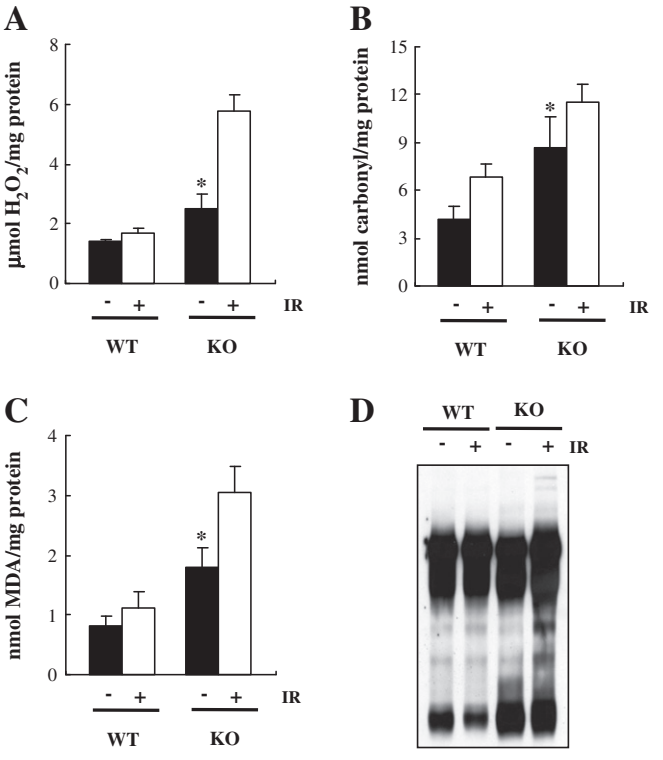

Fig. 4. Redox status and oxidative damage in tumor tissues from $idh2^{+/+}$ and $idh2^{-/-}$ mice. (A) Production of H_2O_2 in tumors from mice exposed to IR was measured with xylenol orange. Each value represents the mean ± S.D. from five to six independent experiments. $^*p < 0.01$ versus non-irradiated $idh2^{+/+}$ mice. (B) Protein carbonyl contents of tumors from mice exposed to IR. The level of protein carbonyls was measured in cell lysates with DNPH. Each value represents the mean ± S.D. from five or six independent experiments. $^*p < 0.01$ versus non-irradiated $idh2^{+/+}$ mice. (C) The level of MDA accumulated in tumor tissue extracts was determined using a TBARS assay. Each value represents the mean ± S.D. from five or six independent experiments. $^*p < 0.01$ versus non-irradiated $idh2^{+/+}$ mice. (D) 4-HNE adducts in the tumor tissue extracts were monitored with an anti-HNE Michael adduct antibody.

These ROS have the potential to damage critical cellular components such as DNA, proteins, and lipids, eventually resulting in physical and chemical damages that may lead to cell death [29]. We demonstrate that IR inhibited tumor growth in both *idh2*$^{+/+}$ and *idh2*$^{-/-}$ mice. Tumor growth was almost completely abrogated in the *idh2*$^{-/-}$ mice after exposure to 5 Gy of IR. Measuring tumor volume and weight is the traditional method for monitoring tumor formation in vivo. However, these factors may not be reflective of tumorigenesis because necrosis and edema are disregarded when making these measurements [30]. A bioluminescent optical imaging system with the Fluc gene has been widely used because of its simple, noninvasive, convenient, and sensitive characteristics [31]. In vivo bioluminescent and pinhole gamma camera images were acquired after subcutaneous inoculation of each mouse with B16F10 cells expressing the Fluc gene. As shown in Fig. 3, bioluminescent signals from the mice reflected tumor growth. Data quantification showed that IDH2 deficiency resulted in a significant inhibition of tumor growth. This growth was further diminished in both *idh2*$^{+/+}$ and *idh2*$^{-/-}$ mice upon exposure to 5 Gy of IR.

3.3. Redox status and oxidative damage to the tumors

The intracellular redox status is generally conducive for cellular growth and proliferation, and has direct and indirect effects on different components of cell death/survival signaling pathways [32]. To determine whether differences in tumorigenesis observed in the *idh2*$^{+/+}$ and *idh2*$^{-/-}$ mice was associated with ROS formation, the levels of intracellular H_2O_2 in the tumor tissues were measured with xylenol orange. As shown in Fig. 4A, a significantly higher level of intracellular H_2O_2 was observed in the tumor tissue of *idh2*$^{-/-}$ mice compared to that of *idh2*$^{+/+}$ mice. The steady-state levels of H_2O_2 were further increased in the tumor tissue of both *idh2*$^{+/+}$ and *idh2*$^{-/-}$ mice following exposure to 5 Gy of IR.

Protein oxidation and lipid peroxidation were also evaluated as markers of oxidative damage to cells. When we measured carbonyl contents to monitor protein oxidation, tumor tissues from the *idh2*$^{-/-}$ mice had an approximately 2-fold increase of carbonyl groups compared to those from *idh2*$^{+/+}$ mice. Protein oxidation was further increased with the exposure of 5 Gy of IR in both *idh2*$^{+/+}$ and *idh2*$^{-/-}$ mice (Fig. 4B). It is well known that oxidative stress in various cells usually leads to the accumulation of cytotoxic lipid peroxides and their breakdown products such as MDA and 4-hydroxynonenal [33]. As shown in Fig. 4C, lipid peroxidation measured as TBARS in the tumor tissue from *idh2*$^{-/-}$ mice was significantly higher than that of the *idh2*$^{+/+}$ mice. Lipid peroxidation was further increased by exposure to 5 Gy of IR in both *idh2*$^{+/+}$ and *idh2*$^{-/-}$ mice. Similar results were also observed for the HNE protein adducts analysis by immunoblotting with an anti-HNE antibody (Fig. 4D).

3.4. Modulation of tumorigenesis marker expression

At higher ROS levels, cell division is stalled and the cells undergo apoptosis after prolonged arrest [34]. p53 becomes activated by oxidative stress, binds to DNA, and activates the expression of several genes including p21, a protein that arrests cancer cells in the G_1 phase and modulates the kinase activities of various cyclin-dependent kinases [35,36]. As shown in Fig. 5A, Western blot analysis revealed that the amount of p21 and phosphorylated p53 was increased in tumor tissues from the *idh2*$^{-/-}$ mice compared to those from *idh2*$^{+/+}$ mice. It was recently demonstrated that the forced expression of cyclin D3 inhibits skin tumorigenesis, indicating that cyclin D3 and cyclin D2 play opposing roles in mouse skin carcinogenesis [37]. The expression of cyclin D3 was markedly increased in tumor tissues from the *idh2*$^{-/-}$ mice compared to those from *idh2*$^{+/+}$ mice.

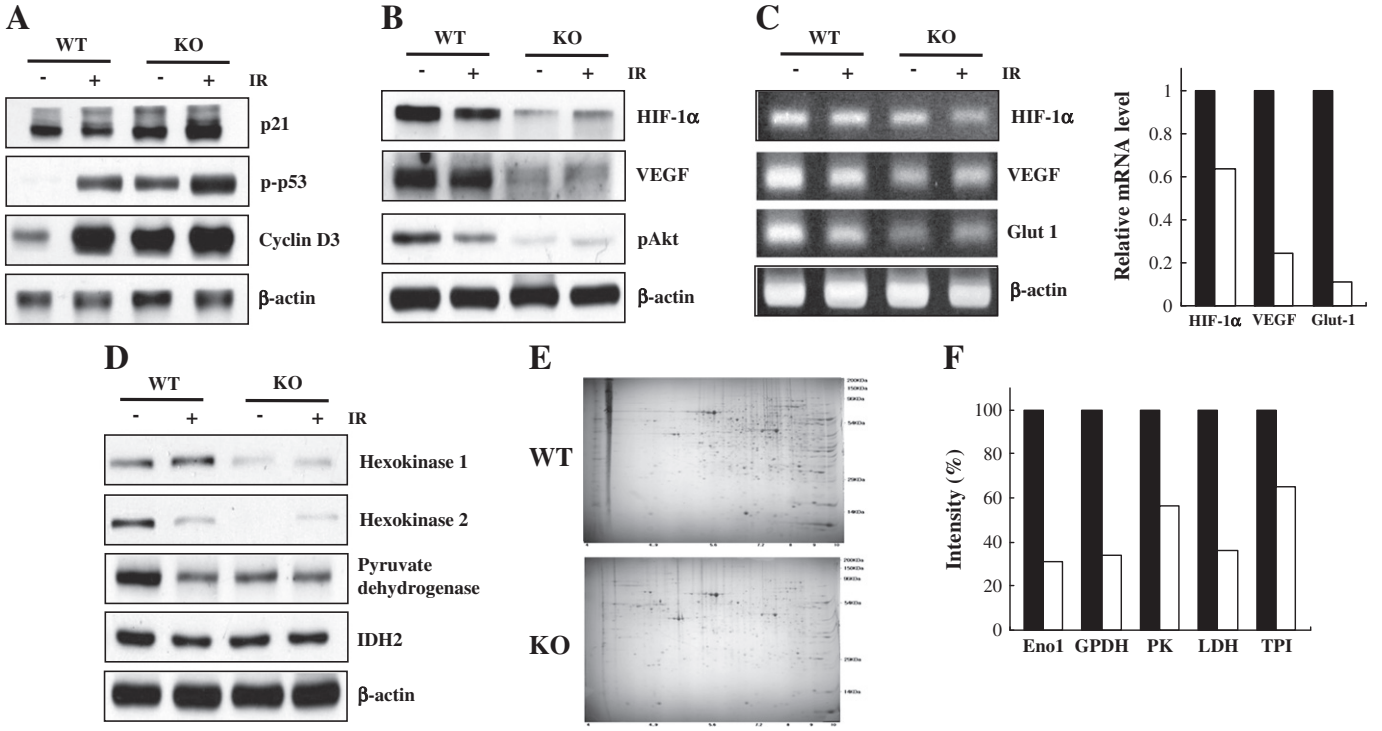

Fig. 5. Modulation of tumorigenesis marker expression in tumor tissues from *idh2*$^{+/+}$ and *idh2*$^{-/-}$ mice. (A) Whole cell extracts of tumor tissues from γ-irradiated mice were subjected to Western blotting to analyze the protein expression of cell cycle markers. (B) Tumor lysates containing equal amounts of protein (20 μg) were separated by SDS-PAGE and then subjected to immunoblot analysis using antibodies specific for angiogenesis markers. (C) Levels of HIF-1α, VEGF, and Glut-1 mRNA were measured by RT-PCR, normalized to β-actin mRNA, and are presented as fold-decrease over the levels observed in *idh2*$^{+/+}$ mice. (D) Tumor lysates containing equal amounts of protein (20 μg) were separated by SDS-PAGE and then subjected to immunoblot analysis using antibodies against glycolytic metabolism factors. (E) 2-DE map of tumor tissues from *idh2*$^{+/+}$ and *idh2*$^{-/-}$ mice. The proteins were extracted, separated on an immobilized pH 4–7 IPG strip, and separated again on a 10–16% polyacrylamide gel. (F) Intensity of spots corresponding to enolase 1, glycerol 3-phosphate dehydrogenase, pyruvate kinase, lactate dehydrogenase, and triosephosphate isomerase in the tumor tissue from *idh2*$^{-/-}$ mice were normalized to those from tumor tissues of *idh2*$^{+/+}$ mice.

Hypoxia-inducible factor-1 (HIF-1) has been identified as a master transcription regulator that holds important roles in development, physiology, and many pathological processes including cancer development [38,39]. Many of the genes that are direct targets of HIF-1α are involved in angiogenesis, metabolic adaptation, apoptosis, and invasion/metastasis [40]. Genetic alterations in signal transduction pathways are highly variable among human tumors, but increased expression of HIF-1α may represent a common final pathway in tumorigenesis [41]. Thus, HIF-1α-mediated angiogenesis and metabolic adaptation may play critical roles in tumor progression. The protein levels of HIF-1α in tumor tissues from *idh2*$^{+/+}$ and *idh2*$^{-/-}$ mice were examined by immunoblotting. HIF-1α accumulation in the tumor tissue from *idh2*$^{-/-}$ mice was significantly reduced compared to that observed in *idh2*$^{+/+}$ mice. Furthermore, tumor tissues from the *idh2*$^{-/-}$ mice had reduced expression of VEGF, a known target of HIF-1α.

The phosphatidylinositol 3-kinase (PI3K)/Akt pathway is constitutively activated in human tumor cells, resulting in increased expression of HIF-1α through activation of Sp1 [42,43]. Akt, a serine-threonine kinase and downstream target of PI3K, is regulated by phosphoinositide-dependent protein kinases (PDKs) [44]. Akt phosphorylation in tumor tissues from the *idh2*$^{-/-}$ mice was significantly reduced compared to those from *idh2*$^{+/+}$ mice (Fig. 5B). Consistent with Western blot analysis showing that tumor tissues from *idh2*$^{-/-}$ mice had significantly decreased HIF-1α expression, blunted mRNA expression of HIF-1α, VEGF, and the glucose transport protein Glut-1 was also observed (Fig. 5C).

A universally observed clinical phenotype of highly malignant tumors is the propensity to rapidly proliferate and spread within a tumor-bearing host [42]. One molecular strategy underlying this characteristic is the tumor's ability to consume glucose at abnormally high rates. The key sub-cellular and molecular players that propel this metabolic transformation can be distilled to a few select enzymes, notably hexokinase and several mitochondria-associated enzymes [45]. As shown in Fig. 5D, a Western blot analysis revealed that the expression levels of hexokinase I, hexokinase II, and pyruvate dehydrogenase were markedly decreased in tumor tissue from the *idh2*$^{-/-}$ mice compared to those from the *idh2*$^{+/+}$ mice.

To further investigate alterations in the expression of genes with roles in glycolytic metabolism, we carried out a proteomic analysis of tumor tissues from the *idh2*$^{+/+}$ and *idh2*$^{-/-}$ mice. Differential proteomic analysis by 2-DE of the soluble protein fraction from the tumor tissues was performed. Representative 2-DE gel images are shown in Fig. 5E. Proteins were subsequently identified by MALDI-TOF MS including key enzymes involved in glycolytic metabolism (Fig. 5F). Down-regulated expression of enolase 1, glycerol 3-phosphate dehydrogenase, pyruvate kinase, lactate dehydrogenase, and triosephosphate isomerase was observed, indicating that the reduction of glycolytic metabolism may be associated with the suppression of tumor growth in the *idh2*$^{+/+}$ mice.

3.5. Modulation of redox status and angiogenesis marker expression in the tumor stroma

The importance of cellular context as a factor that drives tumorigenesis has led to the hypothesis that the stroma surrounding tumors exerts a tissue modification field effect that promotes the development and progression of epithelial malignancies [2,46]. Possible mechanisms underlying the tumor suppression associated with IDH2 deficiency could be enhanced oxidative stress and decreased tumor angiogenesis. Therefore, we attempted to clarify the response of the host microenvironment to metastatic cancer cells. To assess the difference in ROS

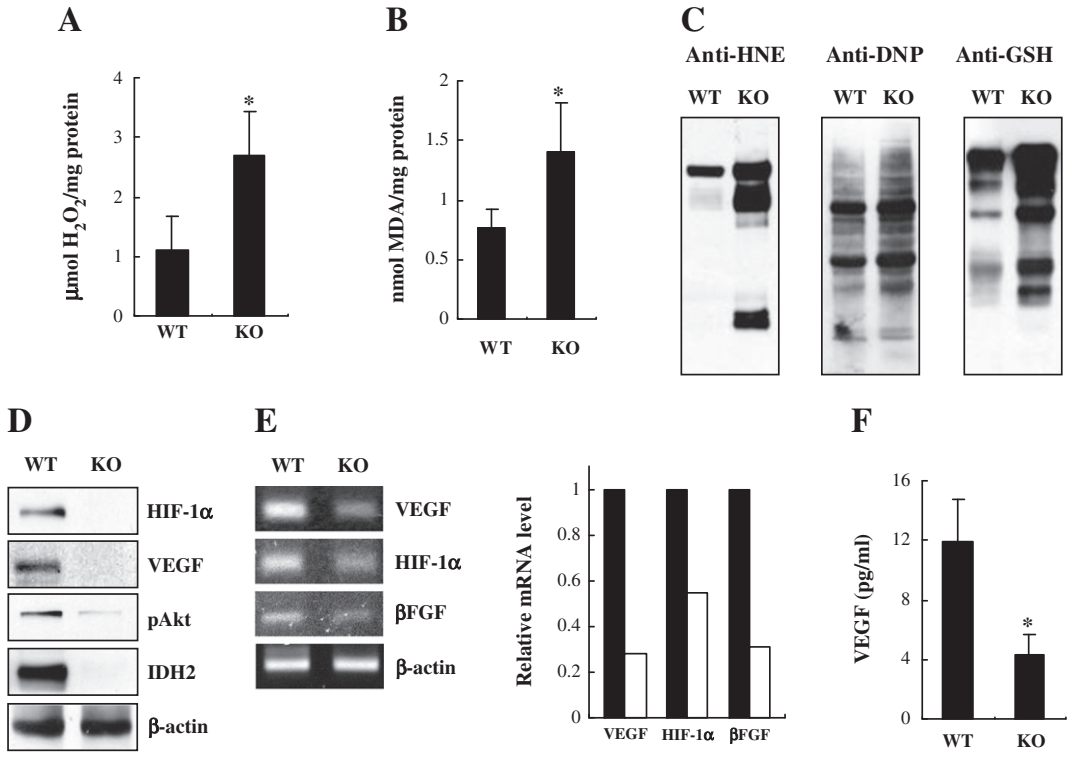

Fig. 6. Modulation of redox status and angiogenesis marker expression in the stroma of *idh2*$^{+/+}$ and *idh2*$^{-/-}$ mice. (A) Production of H_2O_2 in the stroma of the mice was measured with xylenol orange. Each value represents the mean ± S.D. from five or six independent experiments. *$p < 0.01$ versus the *idh2*$^{+/+}$ mice. (B) The level of MDA accumulated in stromal extracts was determined using a TBARS assay. Each value represents the mean ± S.D. from five or six independent experiments. *$p < 0.01$ versus the *idh2*$^{+/+}$ mice. (C) The levels of 4-HNE, DNP, and glutathionylated adducts in the stromal tissue extracts were measured with an anti-HNE Michael adduct antibody, anti-DNP antibody, and anti-GSH antibody, respectively. (D) Stromal lysates containing equal amounts of protein (20 μg) were separated by SDS-PAGE and then subjected to immunoblot analysis using antibodies specific for angiogenesis markers. (E) HIF-1α, VEGF, and βFGF mRNA levels were measured by RT-PCR, normalized to β-actin mRNA, and are presented as fold-decrease over the levels observed in *idh2*$^{+/+}$ mice. (F) The plasma levels of VEGF in *idh2*$^{+/+}$ and *idh2*$^{-/-}$ mice were analyzed using a mouse VEGF ELISA kit. Each value represents the mean ± S.D. from five or six independent experiments. *$p < 0.01$ versus the *idh2*$^{+/+}$ mice.

formation in the $idh2^{+/+}$ and $idh2^{-/-}$ mice, the levels of intracellular H_2O_2 in the stromal tissues were evaluated. As shown in Fig. 6A, IDPm deficiency was accompanied by substantial elevations of intracellular H_2O_2 levels in the stromal tissue measured by xylenol orange.

As indicative markers of oxidative damage to cells, lipid peroxidation and protein oxidation were also evaluated. As shown in Fig. 6B, lipid peroxidation measured as TBARS in the stromal tissue of $idh2^{-/-}$ mice was significantly higher than that of the $idh2^{+/+}$ mice. Similar results were also observed for the HNE protein adduct analysis using an anti-HNE antibody (Fig. 6C). Levels of oxidative protein damage were measured by determining the number of derivatized carbonyl groups on oxidized proteins from the stroma lysates by Western blotting for oxidized protein carbonyl groups. Data from this analysis showed an increase in oxidative protein damage in stromal tissues from the $idh2^{-/-}$ mice compared to those from $idh2^{+/+}$ mice. There are numerous oxidative stress-induced conditions during which the redox status and GSH/GSSG ratio are perturbed [47]. Protein S-glutathionylation is a post-translational modification of protein sulfhydryl groups that occurs under oxidative stress [48]. As shown in Fig. 6C, Western blot analysis of stromal lysates with an anti-GSH IgG revealed a significant increase of glutathionylated proteins in the stroma tissues from $idh2^{-/-}$ mice. Taken together, our findings indicated that excessive production of ROS in the stroma may elicit a bystander effect, leading to oxidative stress and cell death in adjacent cancer cells.

For many cancer treatments, cytotoxic ROS have been extensively used to kill tumor cells that are equipped with a weaker antioxidant defense system than normal cells [9,49]. We sought to characterize the altered expression of factors capable of influencing cancer cell invasion and metastasis. The protein levels of HIF-1α, VEGF, and p-Akt in stromal tissues from $idh2^{+/+}$ and $idh2^{-/-}$ mice were examined by immunoblot analysis. As shown in Fig. 6D, accumulation of these angiogenesis markers in the stromal tissue of $idh2^{-/-}$ mice was significantly reduced compared to that from $idh2^{+/+}$ mice. Consistent with the Western blot results, stromal tissue from the $idh2^{-/-}$ mice also had significantly decreased HIF-1α, VEGF, and βFGF mRNA levels (Fig. 6E). Furthermore, plasma levels of VEGF in the $idh2^{-/-}$ mice were markedly lower compared to those of the $idh2^{+/+}$ mice (Fig. 6F). Taken together, our findings showed that down-regulated expression of angiogenesis markers creates an environment undesirable for tumor survival and growth. Previously, we have shown that inhibition of the PI3K/Akt pathway in IDH2 knockdown cells results in the inhibition of HIF-1α mRNA expression [50].

In summary, we demonstrated that tumorigenesis is suppressed in mice deficient in IDH2, which is accompanied by a significant elevation of oxidative stress and decreased expression of angiogenesis markers in both the tumor and stroma. These results indicate that the process of tumorigenesis may be influenced by interactions between intrinsic alterations of tumor cells and the extrinsic microenvironment. Our findings support the hypothesis that changes of redox status in the stromal microenvironment may contribute to the progression of melanoma neoplasia.

Acknowledgements

This research was supported by the National Research Foundation (NRF) of Korea Grants funded by the Korean Government (201300329, 2013041811 and 2013004950).

References

[1] B. Chen, B.W. Pogue, X. Zhou, J.A. O'Hara, N. Solban, E. Demidenko, P.J. Hoopes, T. Hasan, Effect of tumor host microenvironment on photodynamic therapy in a rat prostate tumor model, Clin. Cancer Res. 11 (2005) 720–727.
[2] C. Bavik, I. Coleman, J.P. Dean, B. Knudsen, S. Plymate, P.S. Nelson, The gene expression program of prostate fibroblast senescence modulates neoplastic epithelial cell proliferation through paracrine mechanisms, Cancer Res. 66 (2006) 794–802.
[3] M.J. Bissell, D. Radisky, Putting tumours in context, Nat. Rev. Cancer 1 (2001) 46–54.
[4] M.M. Mueller, N.E. Fusenig, Friends or foes: bipolar effects of the tumour stroma in cancer, Nat. Rev. Cancer 4 (2004) 839–849.
[5] N.A. Bhowmick, E.G. Neilson, H.L. Moses, Stromal fibroblasts in cancer initiation and progression, Nature 432 (2004) 332–337.
[6] J.A. Joyce, J.W. Pollard, Microenvironmental regulation of metastasis, Nat. Rev. Cancer 9 (2009) 239–252.
[7] K. Polyak, I. Haviv, I.G. Campbell, Co-evolution of tumor cells and their microenvironment, Trends Genet. 25 (2009) 30–38.
[8] J. Wang, J. Yi, Cancer cell killing via ROS, Cancer Biol. Ther. 7 (2008) 1875–1884.
[9] M. Nishikawa, Reactive oxygen species in tumor metastasis, Cancer Lett. 266 (2008) 53–59.
[10] B. Chance, H. Sies, A. Boveris, Hydroperoxide metabolism in mammalian organs, Physiol. Rev. 59 (1979) 527–605.
[11] A.F. Miller, Superoxide dismutases: active sites that save, but a protein that kills, Curr. Opin. Chem. Biol. 8 (2004) 162–168.
[12] D.A. Dickinson, H.J. Forman, Glutathione in defense and signaling: lessons from a small thiol, Ann. N. Y. Acad. Sci. 973 (2002) 488–504.
[13] A.M. Avery, S.A. Willetts, S.V. Avery, Genetic dissection of the phospholipid hydroperoxidase activity of yeast gpx3 reveals its functional importance, J. Biol. Chem. 279 (2004) 46652–46658.
[14] C.E. Outten, V.C. Culotta, Alternative start sites in the *Saccharomyces cerevisiae* GLR1 gene are responsible for mitochondrial and cytosolic isoforms of glutathione reductase, J. Biol. Chem. 279 (2004) 7785–7791.
[15] C.H. Lillig, M.E. Lonn, M. Enoksson, A.P. Fernandes, A. Holmgren, Short interfering RNA-mediated silencing of glutaredoxin 2 increases the sensitivity of HeLa cells toward doxorubicin and phenylarsine oxide, Proc. Natl. Acad. Sci. U. S. A. 101 (2004) 13227–13232.
[16] D.E. Koshland, K. Walsh, D.C. LaPorte, Sensitivity of metabolic fluxes to covalent control, Curr. Top. Cell. Regul. 27 (1985) 13–22.
[17] S.H. Jo, M.K. Son, H.J. Koh, S.M. Lee, I.H. Song, Y.O. Kim, Y.S. Lee, K.S. Jeong, W.B. Kim, J.W. Park, B.J. Song, T.L. Huh, Control of mitochondrial redox balance and cellular defense against oxidative damage by mitochondrial $NADP^+$-dependent isocitrate dehydrogenase, J. Biol. Chem. 276 (2001) 16168–16176.
[18] K. Smolkova, P. Jezek, The role of mitochondrial $NADP^+$-dependent isocitrate dehydrogenase in cancer cells, Int. J. Cell Biol. (2012) 273947(ID).
[19] J.K. Tak, J.W. Park, The use of ebselen for radioprotection in cultured cells and mice, Free Radic. Biol. Med. 46 (2009) 1177–1185.
[20] I.S. Kil, S.Y. Kim, S.J. Lee, J.W. Park, Small interfering RNA-mediated silencing of mitochondrial $NADP^+$-dependent isocitrate dehydrogenase enhances the sensitivity of HeLa cells toward tumor necrosis factor-alpha and anticancer drugs, Free Radic. Biol. Med. 43 (2007) 1197–1207.
[21] C.T. Shearn, P. Reigan, D.R. Petersen, Inhibition of hydrogen peroxide signaling by 4-hydroxynonenal due to differential regulation of Akt1 and Akt2 contributes to decreases in cell survival and proliferation in hepatocellular carcinoma cells, Free Radic. Biol. Med. 53 (2012) 1–11.
[22] M. Arai, H. Imai, T. Koumura, T. Yoshida, K. Emoto, M. Umeda, N. Chiba, Y. Nakagawa, Mitochondrial phospholipid hydroperoxide glutathione peroxidase plays a major role in preventing oxidative injury to cells, J. Biol. Chem. 274 (1999) 4924–4933.
[23] A. Holmgren, Thioredoxin, Annu. Rev. Biochem. 54 (1985) 237–271.
[24] M. Araki, H. Nanri, K. Ejima, Y. Murasato, T. Fujiwara, Y. Nakashima, M. Ikeda, Antioxidant function of the mitochondrial protein SP-22 in the cardiovascular system, J. Biol. Chem. 274 (1999) 2271–2278.
[25] S.W. Kang, H.Z. Chae, M.S. Seo, K. Kim, I.C. Baines, S.G. Rhee, Mammalian peroxiredoxin isoforms can reduce hydrogen peroxide generated in response to growth factors and tumor necrosis factor-alpha, J. Biol. Chem. 273 (1998) 6297–6301.
[26] S. Watabe, H. Hasegawa, K. Takimoto, Y. Yamamoto, S. Takahashi, Possible function of SP-22, a substrate of mitochondrial ATP-dependent protease, as a radical scavenger, Biochem. Biophys. Res. Commun. 213 (1995) 1010–1016.
[27] B. Knoops, A. Clippe, C. Bogard, K. Arsalane, R. Wattiez, C. Hermans, E. Duconseille, P. Falmagne, A. Bernard, Cloning and characterization of AOEB166, a novel mammalian antioxidant enzyme of the peroxiredoxin family, J. Biol. Chem. 274 (1999) 30451–30458.
[28] C. von Sonntag, Free Radical-induced DNA Damage and Its Repair, A Chemical Perspective, Springer, Berlin, 2006.
[29] J.H. Pinthus, I. Bryskin, J. Trachtenberg, J.P. Lu, G. Singh, E. Fridman, B.C. Wilson, Androgen induces adaptation to oxidative stress in prostate cancer: implications for treatment with radiation therapy, Neoplasia 9 (2007) 68–80.
[30] J. Xin, Y. Zhan, M. Liu, H. Hu, L. Xia, Y. Nie, K. Wu, J. Liang, J. Tian, ApoG2 induces ER stress-dependent apoptosis in gastric cancer cells in vitro and its real-time evaluation by bioluminescence imaging in vivo, Cancer Lett. 336 (2013) 260–269.
[31] J.H. Kang, J.K. Chung, Molecular-genetic imaging based on reporter gene expression, J. Nucl. Med. 49 (2008) 164S–179S.
[32] D. Trachootham, W. Lu, M.A. Ogasawara, R.D. Nilsa, P. Huang, Redox regulation of cell survival, Antioxid. Redox Signal. 10 (2008) 1343–1374.
[33] H. Esterbauer, R.J. Schaur, H. Zollner, Chemistry and biochemistry of 4-hydroxynonenal, malonaldehyde and related aldehydes, Free Radic. Biol. Med. 11 (1991) 81–128.
[34] W.C. Burhans, N.H. Heintz, The cell cycle is a redox cycle: linking phase-specific targets to cell fate, Free Radic. Biol. Med. 47 (2009) 1282–1293.
[35] A. Zetterberg, O. Larsson, K.G. Wiman, What is the restriction point? Curr. Opin. Cell Biol. 7 (1995) 835–842.
[36] Y. Yu, Z. Kovacevic, D.R. Richardson, Tuning cell cycle regulation with an iron key, Cell Cycle 6 (2007) 1982–1994.
[37] P. Rojas, M.B. Cadenas, P.C. Lin, F. Benavides, C.J. Conti, M.L. Rodriguez-Puebla, Cyclin D2 and cyclin D3 play opposite roles in mouse skin carcinogenesis, Oncogene 26 (2007) 1723–1730.
[38] G. Melillo, HIF-1: a target for cancer, ischemia and inflammation—too good to be true? Cell Cycle 3 (2004) 154–155.

[39] G.L. Semenza, Targeting HIF-1 for cancer therapy, Nat. Rev. Cancer 3 (2003) 721–732.
[40] F. Li, P. Sonveaux, Z.N. Rabbani, S. Liu, B. Yan, Q. Huang, Z. Vujaskovic, M.W. Dewhirst, C.Y. Li, Regulation of HIF-1α stability through S-nitrosylation, Mol. Cell 26 (2007) 63–74.
[41] H. Zhong, K. Chiles, D. Feldser, E. Laughner, C. Hanrahan, M.M. Georgescu, J.W. Simons, G.L. Semenza, J.W. Simons, Modulation of hypoxia-inducible factor 1alpha expression by the epidermal growth factor/phosphatidylinositol 3-kinase/PTEN/AKT/FRAP pathway in human prostate cancer cells: implications for tumor angiogenesis and therapeutics, Cancer Res. 60 (2000) 1541–1545.
[42] J.E. Thompson, C.B. Thompson, Putting the rap on Akt, J. Clin. Oncol. 22 (2004) 4217–4226.
[43] B.H. Jiang, G. Jiang, J.Z. Zheng, Z. Lu, T. Hunter, P.K. Vogt, Phosphatidylinositol 3-kinase signaling controls levels of hypoxia-inducible factor 1, Cell Growth Differ. 12 (2001) 363–369.
[44] D.R. Alessi, S.R. James, C.P. Downes, A.B. Holmes, P.R. Gaffney, C.B. Reese, P. Cohen, Characterization of a 3-phosphoinositide-dependent protein kinase which phosphorylates and activates protein kinase Bα, Curr. Biol. 7 (1997) 261–269.
[45] S.P. Mathupala, Y.H. Ko, P.L. Pedersen, The pivotal roles of mitochondria in cancer: Warburg and beyond and encouraging prospects for effective therapies, Biochim. Biophys. Acta 1797 (2010) 1225–1230.
[46] H.Y. Chang, J.B. Sneddon, A.A. Alizadeh, R. Sood, R.B. West, K. Montgomery, J.T. Chi, M. van de Rijn, D. Botstein, P.O. Brown, Gene expression signature of fibroblast serum response predicts human cancer progression: similarities between tumors and wounds, PLoS Biol. 2 (2004) E7.
[47] S. Bharath, M. Hsu, D. Kaur, S. Rajagopalan, J.K. Andersen, Glutathione, iron and Parkinson's disease, Biochem. Pharmacol. 64 (2002) 1037–1048.
[48] Y.C. Chai, S.S. Ashraf, K. Rokutan, R.B. Johnston, J.A. Thomas, S-thiolation of individual human neutrophil proteins including actin by stimulation of the respiratory burst: evidence against a role for glutathione disulfide, Arch. Biochem. Biophys. 310 (1994) 273–281.
[49] A. Laurent, C. Nicco, C. Chéreau, C. Goulvestre, J. Alexandre, A. Alves, E. Lévy, F. Goldwasser, Y. Panis, O. Soubrane, B. Weill, F. Batteux, Controlling tumor growth by modulating endogenous production of reactive oxygen species, Cancer Res. 65 (2005) 948–956.
[50] S.Y. Kim, J.W. Park, Modulation of hypoxia-inducible factor-1α expression by mitochondrial $NADP^+$-dependent isocitrate dehydrogenase, Biochimie 92 (2010) 1908–1913.